Title: Analysis of biomechanical stresses caused by hindfoot joint arthrodesis in the treatment of adult acquired flatfoot deformity: A finite element study

Authors: Christian Cifuentes-De la Portilla, Ricardo Larrainzar-Garijo, Javier Bayod

PII: S1268-7731(19)30073-6
DOI: https://doi.org/10.1016/j.fas.2019.05.010
Reference: FAS 1311

To appear in: *Foot and Ankle Surgery*

Received date: 15 January 2019
Revised date: 9 May 2019
Accepted date: 13 May 2019

Please cite this article as: Cifuentes-De la Portilla C, Larrainzar-Garijo R, Bayod J, Analysis of biomechanical stresses caused by hindfoot joint arthrodesis in the treatment of adult acquired flatfoot deformity: A finite element study, *Foot and Ankle Surgery* (2019), https://doi.org/10.1016/j.fas.2019.05.010

Analysis of biomechanical stresses caused by hindfoot joint arthrodesis in the treatment of adult acquired flatfoot deformity: A finite element study

Christian Cifuentes-De la Portilla [a,c], Ricardo Larrainzar-Garijo [b1], Javier Bayod [a]

[a] Applied Mechanics and Bioengineering Group (AMB), Aragón Institute of Engineering Research (I3A), Universidad de Zaragoza, Spain. [b]Orthopaedics and Trauma Department, Medicine School. Universidad Complutense- Hospital Universitario Infanta Leonor, Madrid, Spain. [c] Facultad de Ciencias Médicas - Departamento de Medicina, Universidad Espíritu Santo – Ecuador

[1] Corresponding autor: crisjavri@gmail.com

Highlights

- Biomechanical stress generated by the hindfoot joints arthrodesis was calculated
- Subtalar arthrodesis is the procedure that contributes least to stress reduction
- Talonavicular arthrodesis generates a significant stress reduction in hindfoot
- Calcaneocuboid arthrodesis reduces both the soft tissue and metatarsals stresses
- Triple arthrodesis generates the least tissue stresses in all the evaluated cases

Abstract:

Background: Treatments of adult acquired flatfoot deformity in early stages (I-IIa-IIb) are focused on strengthening tendons, in isolation or combined with osteotomies, but in stage III, rigidity of foot deformity requires more restrictive procedures such as hindfoot joint arthrodesis. Few experimental studies have assessed the biomechanical effects of these treatments, because of the difficulty of measuring these parameters in cadavers. Our objective was to quantify the biomechanical stress caused by both isolated hindfoot arthrodesis and triple arthrodesis on the main tissues that support the plantar arch.

Methods: An innovative finite element model was used to evaluate some flatfoot scenarios treated with isolated hindfoot arthrodesis and triple arthrodesis.

Results and conclusions: When arthrodeses are done in situ, talonavicular seems a good option, possible superior to subtalar and at least equivalent to triple. Calcaneocuboid arthrodesis reduces significantly both fascia plantar and spring ligament stresses but concentrates higher stresses around the fused joint.

Keywords: Arthrodesis, Biomechanics, FE Modeling, Flatfoot, Tibialis tendon dysfunction.

1. Introduction

Adult acquired flatfoot deformity (AAFD[1]) causes a progressive flattening of the foot arch, which has traditionally been associated with tibialis posterior tendon (TPT) dysfunction [1,2,3]. However, some clinical studies have found that the failure or rupture of the plantar

[1]AAFD: Adult acquired flatfoot deformity, TPT: Tibialis posterior tendon, PF: Plantar fascia, SL: Spring ligament, PBT: Peroneus brevis tendon, PLT: Peroneus longus tendon, LPL: Long plantar ligament, SPL: Short plantar ligament, FDL: Flexor digitorum ligament, FHL: Flexor hallucis ligament.

fascia (PF) or the calcaneonavicular ligament (known as the Spring ligament (SL)) could also generate both the collapse of the arch and forefoot abduction, the main signs of AAFD [1,4,5]. In the early stages of the disease (Stages I, IIa and IIb), many treatment options focus on strengthening the TPT, in isolation or combined with some osteotomies, to rebalance the foot structure. However, when the flatfoot deformity is rigid (stage III or IV), surgeons need to use more restrictive treatments such as arthrodesis of the hindfoot joints (subtalar, talonavicular and calcaneocuboid) in isolation or combined (triple arthrodesis or other procedures) [6,7,8]. Isolated posterior subtalar arthrodesis is a well-known procedure used to treat AAFD when the foot arch has a rigid deformation or signs of joint instability, arthritis and pain [9]. A cadaver model-based study that compares the capacity of maintaining the foot arches after applying different hindfoot joint arthrodeses found that isolated posterior subtalar arthrodesis was less effective in supporting both medial and longitudinal arches compared to calcaneocuboid and talonavicular arthrodeses [10]. On the other hand, some studies show that isolated talonavicular arthrodesis has notable advantages, especially in pain control. Harper et al. [11] carried out a follow - up study (26 months) of 29 patients treated with a talonavicular arthrodesis, finding good results in about 86% of the cases. However, this arthrodesis has also been associated with an increased risk of malunion, pseudarthrosis and progressive osteoarthritis in adjacent joints (in about 3% to 10% of treated patients) [12]. Calcaneocuboid arthrodesis is a procedure commonly applied in conjunction with other procedures (including lateral column lengthening) and is rarely performed in isolation. Some studies have found that the isolated arthrodesis of the calcaneocuboid joint causes degenerative arthritis signs in the surrounding joints [13], including also pseudarthrosis, non-union and stress fracture of the lateral column of the foot. Additionally, there is also evidence that it affects walking on

rough surfaces [13]. Nevertheless, some success cases have also been reported in patients with an isolated fusion of the calcaneocuboid joint [14,15]. Finally, triple arthrodesis is perhaps one of the most commonly used surgical procedures in AAFD correction in both the intermediate and advanced stages [16]. Surgeons may consider triple arthrodesis when tendon reinforcement procedures or an isolated hindfoot arthrodesis fail [16,17]. Over time, this procedure has proved to be a reliable and reproducible alternative for the successful correction of the foot structure deformity with good clinical results. However, long-term follow-up of patients has shown that many of them develop arthritis around the ankle, and pain in the midfoot and toes [16,17,18].

All the available information is based on subjective evidence of the side-effects of these procedures (especially related with pain and arthrosis), because it is extremely difficult to measure tissue stresses in isolation in experimental tests with consistent results [19]. An alternative approach nowadays accepted by clinicians and biomedical engineers is finite element (FE) modeling. This computational methodology allows the design of complex models that adequately represent the biomechanics of the human foot [20,21]. Many models have been reported for studying foot biomechanics and the effects of some surgical procedures. However, these models are focused specifically on foot structure deformation and plantar pressure measurement [20], simplifying the soft tissue anatomy. This strong simplification does not allow the measurement of relevant biomechanical aspects such as the tissue traction stress, limiting the information required to understand the mechanical consequences of altering the normal foot structure by fusing the hindfoot joints [22].

The objective of this study was to use a finite element foot model to quantify the biomechanical stress caused by isolated complete subtalar, talonavicular or calcaneocuboid arthrodeses and triple arthrodesis on both foot bones and the main soft tissues that stabilize the longitudinal arch. Our hypothesis is that this analysis strategy could identify some hidden biomechanical effects of these arthrodeses, as well as finding differences and similarities that might give surgeons new information to decide the best treatment option, depending on both the signs and severity of the flatfoot deformity. The analysis was performed simulating a TPT dysfunction and a severe case simulated combining TPT, PF and SL failures, applying in all cases the arthrodeses mentioned.

2. Material and methods

2.1. Finite element model design

This model reconstructs a healthy human unloaded foot, based on CT-images (radiographs to 0.6 mm/slide) acquired from the right foot of a 49-year-old man (weight = 75 Kg, height = 1.70 m). Tissue segmentation and 3-D reconstruction (Bones, PF, TPT, Achilles tendon (AT) and peroneus longus tendon (PLT), peroneus brevis tendon (PBT), flexor digitorum longus (FDL), flexor hallucis longus (FHL)) were performed using MIMICS V. 10 (Materialize, Leuven, Belgium). The model maintains the cartilage morphology as well as the differentiation between cortical and trabecular bone. This characteristic is important when biomechanical stress is evaluated, even though some authors have simplified the bone structure by characterizing the bone tissue as completely cortical or considering an average of the mechanical properties of both cortical and trabecular bone [23,24,25]. Because of the difficulty of segmenting the SL and both the short plantar

ligament (SPL) and the long plantar ligament (LPL) from images, these tissues were added to the model through the reconstruction of their anatomy following both body atlas and surgeons' guidance. The complete FE model is shown in fig. 1.

2.2. Meshing

The model's meshing was performed using ICEM CFD V. 15 software (Canonsburg, Pennsylvania, United States), generating 28 cortical bone pieces, 24 trabecular bone pieces, 26 cartilage segments, 4 tendons, 3 ligaments and the plantar fascia. A trial-error approach was employed to optimize the mesh size of each segment, following the recommendations of Burkhart et al. [26] who suggest that in all the parameters measured, the number of inaccurate elements must be less than 5% (see table 1). All simulations and post-processing were performed in Abaqus/CAE 6.14 (Dessault Systémes, Vélizy-Villacoublay, France) using the Nonlinear geometry solver available.

2.3. Tissue biomechanical properties and arthrodeses simulation

Tissue properties (Young's modulus and Poisson's ratio) of the cortical bone, trabecular bone, ligaments and plantar fascia were assigned in accordance with published data [23,19]. The tendons and cartilages were modeled as hyper-elastic materials (Ogden model), using the parameters used in specialized articles [27,28]. The tissue failures or weakness applied to simulate AAFD development were performed applying the Isotropic Hardening theory that generates a progressive tissue weakening.

To simulate each case of arthrodesis, the cartilage tissues of the fused joint were replaced with cortical bone (Fig. 2) in order to emulate a complete joint union. These changes were performed before starting the simulations (unloaded foot). No external fixation elements were included.

2.4. Loading and Boundary conditions:

The model was reconstructed from CT-images of an unloaded foot (Internal Moreau-Costa-Bertani angle (IMCB) of 106°). The first step was to generate a normal standing load position (midstance) for use as a reference case and for comparison with all the simulated cases of both AAFD and surgical procedures. All simulations were performed applying the loading and boundary conditions shown in fig. 3. The load of 720N represents the full weight of an adult of about 73Kg, leaning on one foot, which emulates a traditional scenario of an AAFD diagnosis assessment.

The load was included in a descending vertical direction and 10 degrees of inclination, distributed as follows: Tibia – Talus joint (90%) and Fibula – Talus (10%) [29]. The tendon traction force was included as reported by Arangio et al. [30]. All simulations were performed maintaining fixed nodes at the lower part of the calcaneus and blocking the Z-axis displacement (vertical) of the lower nodes of the first and fifth metatarsals. In this way, the ground effect in the midstance phase was simulated.

To obtain the flatfoot deformation, the model was first simulated removing the TPT traction force [31]. Then a severe case was simulated, adding the weakening of both PF and SL tissues.

2.5. Model Validation

The model was validated following the recommendations of Tao et al. [32]. They measured the vertical displacements of some anatomical points in two different loading conditions: light loading and normal stance loading, using lateral Rx images (Sagittal plane). The variation of these points in each case allowed us to compare the vertical

relative displacements observed in the radiographic images versus those generated by the model. The vertical distance from the ground to the highest point of the talus (TAL) and the navicular (NAV), the midpoint of the first cuneiform (CUN) and the highest point of the first metatarsal head (1MT) was measured, as can be seen in fig. 4. These measurements were taken from images of 12 healthy patients, in order to obtain an average of normality and a standard deviation (SD). The free software “ImageJ” was used to measure the image distances. Each radiological image was obtained at the same distance and was aligned using as reference points the highest point of the talus head, the posterior extreme of the first distal phalanx and the anterior extreme of the calcaneus. Additionally, some foot structural measurements were performed: The IMCB angle, the talocalcaneal divergence (TCD) angle and the Forefoot Abduction (FA) angle.

2.6. Model analysis and evaluation criteria.

The biomechanical stress was quantified using the field output spectrum available in Abaqus/CAE. The parameter used for the evaluation was the maximum principal stress (S. Max). These eigenvalues are closely related to the tensile stress that is generated in foot tissues during normal stance phase. When a dysfunctional soft tissue was included in the simulation, its biomechanical stress was not measured.

3. Results

3.1. About the model validation

Results of the validation process can be seen in table 2. The model generates a foot structure deformation similar to a healthy patient in a loading test, simulating all the tissues in normal and functional conditions. The evaluation was performed observing the foot

anatomy in a sagittal plane under two load conditions: light loading and a normal standing loading.

Additionally, the deformation predicted by the model for a healthy foot generates angles within normal values: IMCB angle of 115 °, an FA angle of 17 ° and a TCD angle of 18° [33].

3.2. About the flatfoot simulation

The foot model developed the main AAFD signs: the too many toes sign, foot arch lengthening, hindfoot pronation and increased forefoot abduction (See fig. 5). Additionally, the structural angles were measured, obtaining: IMCB = 120°, TCD = 24° and FA = 24°.

3.3. Soft tissue stress analysis:

As mentioned above, the first simulations were performed removing the TPT traction force but maintaining both the PF and SL tissues in healthy conditions. Results of the biomechanical stresses of both the PF and SL are shown in fig. 6 and fig. 7, respectively; and the maximum stress generated in the plantar ligaments, peroneus tendons, both flexors digitorum and hallucis longus tendons, and the Achilles tendon are summarized in table 3. Figures shown in this section present a quantification of the stress generated and its localization in the tissue anatomy. The color scale is organized in ascending order: blue represents low stresses, green represents medium stresses, while orange and red represent high stresses. The color scale was normalized to visualize better the differences between cases to 20 N/mm^2 for PF and 30 N/mm^2 for SL. The maximum stress value generated appears in the upper part of the color scale, but in the SL results for both the

calcaneocuboid arthrodesis and triple arthrodesis, the maximum value is presented explicitly because the stress value is less than 30 MPa. The results of the other tissues are summarized in table 3.

3.4. Bone stresses analysis:

In this case, the flatfoot simulation was performed weakening both the PF and SL tissues and removing the TPT traction force. The stresses were measured for hindfoot bones (fig. 7) and forefoot bones (fig. 8), quantifying the maximum principal stress in N/ $N/mm^{2.}$ Results were normalized to 20 N/mm^2 (hindfoot bones) and 100 N/mm^2 (forefoot), to visualize better the stress differences.

It is important to mention that the high stress values generated in the lower part of the calcaneus were caused by the fixed nodes, which prevent the structure displacement during the loading step and allow the model convergence. This is a common problem of stress concentration, a side-effect of the boundary conditions used in the finite element modeling. However, although this condition increases the maximum stress values presented in the color scale, it does not affect the relationship of differences generated between stresses, because this condition is present in all the cases.

Additionally, the maximum principal stress of all the other soft tissues included in the model were calculated. The maximum values are summarized in table 4, presented in units of N/mm^2.

4. Discussion

This study aimed to quantify the stresses in both soft tissues and bones that are generated by isolated arthrodeses (subtalar, talonavicular and calcaneocuboid) and triple arthrodesis, in two pathological scenarios associated to AADF development [1,2], using a detailed finite element model [24,25]. This model generates the most notable AAFD signs: foot arch lengthening, an increase of forefoot abduction and hindfoot pronation. Some authors have proposed computational models to evaluate AAFD. Gefen et al. [34] and later Chaung and Zhang [35] developed models that allow the biomechanical consequences of a complete and partial removal of the PF to be evaluated. Subsequently, Tao et al. [19] developed a detailed FE model with which the contribution of the PF, SL, SPL and LPL to the maintenance of the foot arch was calculated. However, in contrast to our proposal, these models do not consider the cortical and trabecular bone differentiation, nor the tissue geometry needed to perform an accurate stress study. They consider tendons and ligaments as simple bar elements (unidimensional) that generate similar foot structure deformations, but they cannot accurately measure the biomechanical stress values nor their distribution in tissues. There are also computational models used to study foot surgeries, but these maintain the soft tissue simplification mentioned above, reducing their clinical interest for AAFD research [30,36,37].

Experimental studies and patient case reports published in the clinical literature about arthrodeses applied as treatment for AAFD generally suggest that these surgical techniques generate good results, mainly in terms of pain reduction and foot structure correction. However, some side-effects have also been reported associated with pseudarthrosis, metatarsalgia and pain in the joints around the fused region [16,17,38]. Some clinical studies show that a well-fixed arthrodesis will result in normal physiological

contact pressures and will prevent attenuation of the medial soft tissue and consequent degenerative changes [39]. However, inevitably the structural changes caused by the arthrodesis generate additional stresses on soft tissues, joints and bones above and below the fused areas [38].

The results herein presented show that when a TPT dysfunction occurs and an isolated complete subtalar arthrodesis is applied, the PF stress decreases only about 7%, but the SL stress was reduced by 40%. In the same scenario, isolated calcaneocuboid arthrodesis obtained the best decrease in both the PF and SL stress (21% and 72%, respectively). However, the triple arthrodesis obtained the best decrease rates in both PF and SL stresses, almost completely discharging the SL tissue (stress reduction of 89%) and reducing the PF stress by about 30%. Both subtalar and talonavicular arthrodeses were the isolated procedures that obtained the best stress reduction in both FHL and FDL. Talonavicular arthrodesis stands out reducing the LPL stress, while calcaneocuboid arthrodesis notably reduces the SPL. However, this last procedure generates a high increase in both LPL and PLT. Similar results were obtained in the triple arthrodesis simulation. None of the analyzed surgical procedures showed any significative effect on either AT or PBT stress. These results match those obtained by Chen et al. [10] in a study performed using cadaver foot models and by Wong et al. through a computational study [22]. Both found that isolated posterior subtalar arthrodesis is the least effective for correcting the plantar arch structure and the forefoot abduction when a TPT dysfunction occurs.

The second part of this study was focused on an analysis of the biomechanical stress generated on the foot bones. The model was simulated weakening the tissue for both the PF and the SL and removing the TPT traction force. This severe condition allowed us to analyze the stress in all the soft tissues not altered, and also the traction stress differences on both the forefoot and hindfoot bones in all the simulated procedures. The results for the soft tissues stress in this case are similar to those described above. This means that both calcaneocuboid arthrodesis and triple arthrodesis produce a significant reduction in the SPL traction stress but increase the LPL stress even more than the flatfoot scenario. Again, both subtalar and navicular arthrodeses produce the best reduction in the stress on the PLT when TPT weakness was simulated. However, with a failure of PF, SL and TPT, triple arthrodesis shows the higher stress reduction for this tissue, as was expected. Again, none of the procedures show relevant biomechanical effects on either the PBT or the AT because the relationship of these tissues with the plantar arch support is minimal.

The results in fig. 8 show a remarkable stress concentration in the calcaneocuboid joint after applying arthrodesis in this area. These results are similar to those reported by Logel et al. [40] who found a pressure increase on the calcaneocuboid joint and signs of pseudarthrosis and degenerative processes around this area in patients treated with calcaneocuboid arthrodesis both isolated and combined with other surgical techniques. Both isolated talonavicular arthrodesis and triple arthrodesis generated the lowest stress values in hindfoot bones (decreases of 16% and 21%, respectively). Regarding evaluation in the metatarsal bones, the stress increase is notable in all the simulated arthrodesis cases. However, both triple arthrodesis and isolated talonavicular arthrodesis stand out, reducing the metatarsal stress by about 29% and 34 %, respectively, with respect to the

flatfoot case. Summarizing all the results, we observe that isolated calcaneocuboid and triple arthrodesis are the procedures that best reduce the stress in the main passive foot arch stabilizers; while isolated talonavicular and, again, triple arthrodesis are the procedures that generated the least stress in foot bones and joints.

Triple arthrodesis, the results of which stand out in this study, has been demonstrated to be a reliable and reproducible option for successfully correcting foot structure deformity with good clinical results [18]. However, this is a procedure with some defects. Long-term follow-up of patients after triple arthrodesis has shown that many of them develop arthritis or pain around the ankle, midfoot and lateral metatarsals [18]. These changes can take years or even decades to develop, and indeed may never become evident [17]. This fact has motived the search for alternative procedures, a little bit less restrictive. The results of this article suggest that if the rigidity of the arch is not too severe, and there is no evidence of pain or osteoarthritis around other hindfoot joints, an isolated talonavicular arthrodesis might give better results than an isolated subtalar arthrodesis (better stress reduction in soft tissues and less stress in foot bones and joints), which could be combined with other tendon reinforcement procedures or osteotomies, as an alternative to correct flatfoot deformity, keeping most of the joint movements possible.

Finally, we consider that the main limitation of our model is that all the arthrodeses analyzed were simulated in the model "in situ" considering a rigid deformity forefoot which represents that we had canceled the motion between the different joints through an algorithm. We must state that performing any 3D correction arthrodeses the results obtained between the talonavicular and isolated posterior subtalar may be similar in terms

of mechanical effect. Each arthrodesis was simulated as a complete joint-fusion before starting the simulation (unloaded foot in normal position), without including any external support element. However, since our objective was to quantify stress changes generated by the surgical procedures and not the structural correction that each procedure is capable of generating, the initial position of the foot structure is not a determinant. Additionally, although the values of biomechanical stress generated cannot be assumed as true stress values for all people (because of inter-subject variability), we can analyze the relative differences generated in each case and the location of the stress concentration points. Besides, our model was designed from CT-images of an unloaded foot (taken from a traditional radiological foot study), and the initial bone shapes come from a healthy person. Despite these limitations, mainly related with the methodology applied, our study quantified the stresses in foot tissues that cannot be measured in cadavers nor in vivo. This information could improve the understanding of the soft tissue and bone stresses related with both AAFD development and the surgical treatments applied.

5. Conclusions:

The results show that in rigid deformities, when arthrodeses are done “in situ”, Talonavicular arthrodesis is a good option. It generates significant stress reduction and offers an alternative to isolated subtalar arthrodesis and could be combined with other surgical procedures in order to correct flatfoot deformity. In this theoretically situation, subtalar arthrodesis is the isolated hindfoot arthrodesis that contributes least to stress reduction on both the plantar fascia and the spring ligament. In fact, this isolated arthrodesis generates the highest stress on both the forefoot and hindfoot of all the evaluated isolated procedures. Additionally, although calcaneocuboid arthrodesis

significantly reduces the stress in the plantar arch stabilizer tissues, it generates a significant stress concentration that could result in arthritis problems around the fused zone. Triple arthrodesis was the procedure that best reduces the stresses in both soft tissues and foot bones.

Acknowledgments

The authors gratefully acknowledge the support of the Ministry of Economy and competitiveness of the Government of Spain through the project DPI2016-77016-R.

References

[1] Mostafa M. Abousayed, Maxwell C. Alley, Rachel Shakked, and Andrew J. Rosenbaum, "Adult-Acquired Flatfoot Deformity: Etiology, Diagnosis, and Management," JBJS reviews, vol. 5, p. e7, 2017.

[2] Steven L. Haddad et al., "Adult acquired flatfoot deformity," Foot & ankle international, vol. 32, pp. 95-101, 2011.

[3] Jonathan T. Deland, "Adult-acquired Flatfoot Deformity," Journal of the American Academy of Orthopaedic Surgeons, vol. 16, pp. 399-406, 2008.

[4] Jonathan T. Deland, "The adult acquired flatfoot and spring ligament complex: pathology and implications for treatment," Foot and ankle clinics, vol. 6, pp. 129-135, 2001.

[5] L. Herráiz Hidalgo et al., "Disfunción del tendón tibial posterior: ¿qué otras estructuras están implicadas en el desarrollo del pie plano adquirido del adulto?," Radiología, vol. 56, pp. 247-256, 2014.

[6] Eric M. Bluman, Craig I. Title, and Mark S. Myerson, "Posterior Tibial Tendon Rupture: A Refined Classification System," Foot and Ankle Clinics, vol. 12, no. 2, 2007.

[7] Richard G. Alvarez, Andrew Marini, Coleen Schmitt, and Charles L. Saltzman, "Stage I and II posterior tibial tendon dysfunction treated by a structured nonoperative management protocol: an orthosis and exercise program," Foot \& ankle international, vol. 27, pp. 2-8, 2006.

[8] Ana Marchena, Marta Cortés, and Gabriel Gijón Noguerón, "Revisión bibliográfica de los tratamientos del pie plano flexible. Análisis retrospectivo (1977-2011)/Systematic review of flexible flatfoot treatments. Retrospective analysis (1977-2011)," Revista Internacional de Ciencias Podológicas, vol. 7, p. 9, 2013.

[9] G. A. Arangio, K. L. Reinert, and E. P. Salathe, "A biomechanical model of the effect of subtalar arthroereisis on the adult flexible flat foot," Clinical Biomechanics, vol. 19, no. 8, pp. 847-852, 2004.

[10] Y. Chen, K. Zhang, M. Qiang, and Y. & Hao, "Maintenance of longitudinal foot arch after different mid/hind-foot arthrodesis procedures in a cadaveric model.," Clinical Biomechanics, vol. 29, pp. 170-176, 2014.

[11] Marion C. Harper, "Talonavicular arthrodesis for the acquired flatfoot in the adult.," Clinical orthopaedics and related research, pp. 65-68, 1999.

[12] G. M. Weinraub and M. A. Heilala, "Isolated talonavicular arthrodesis for adult onset flatfoot deformity/posterior tibial tendon dysfunction," Clinics in podiatric medicine and surgery, vol. 24, no. 4, pp. 745-752, 2007.

[13] M. Barmada, H. S. Shapiro, and S. F. Boc, "Calcaneocuboid arthrodesis," Clinics in podiatric medicine and surgery, vol. 29, no. 1, pp. 77-89, 2012.

[14] T.J. Chang and D.J. Soomekh, "Lateral column fusions," Clin Podiatr Med Surg, vol. 21, no. 1, pp. 29–39, 2004.

[15] J. Y. Chan et al., "Contribution of lateral column lengthening to correction of forefoot abduction in stage IIb adult acquired flatfoot deformity reconstruction," Foot & ankle international, vol. 36, pp. 1400-1411, 2015.

[16] S. C. Graves, R. A. Mann, and K. O. & Graves, "Triple arthrodesis in older adults. Results after long-term follow-up," JBJS, vol. 75, pp. 355-362, 1993.

[17] I. B. Groot, M. Reijman, H. A. Luning, and J. A. & Verhaar, "Long-term results after a triple arthrodesis of the hindfoot: function and satisfaction in 36 patients," International orthopaedics, vol. 32, pp. 237-241, 2008.

[18] M. Knupp, S. A. Stufkens, and B Hintermann, "Triple arthrodesis," Foot and ankle clinics, vol. 16, no. 1, pp. 61-67, 2011.

[19] Kai Tao, Wen-Ting Ji, Dong-Mei Wang, Cheng-Tao Wang, and Xu Wang, "Relative contributions of plantar fascia and ligaments on the arch static stability: a finite element study," Biomedizinische Technik/Biomedical Engineering, vol. 55, pp. 265-271, 2010.

[20] Yan Wang, Duo Wai-Chi Wong, and Ming Zhang, "Computational models of the foot and ankle for pathomechanics and clinical applications: a review," Annals of biomedical engineering, vol. 44, pp. 213-221, 2016.

[21] Marco Viceconti, Sigbjorn Olsen, Lutz-P. Nolte, and Kim Burton, "Extracting clinically relevant data from finite element simulations," Clinical Biomechanics, vol. 20, pp. 451-454, 2005.

[22] Duo Wai-Chi Wong, Yan Wang, Tony Lin-Wei Chen, Ming Zhang, and A Leung, "Biomechanical consequences of subtalar joint arthroereisis in treating posterior tibial tendon dysfunction: a theoretical analysis using finite element analysis," Computer methods in biomechanics and biomedical engineering, vol. 20, no. 14, pp. 1525-1532, 2017.

[23] J. M. Garcia-Aznar et al., "Load transfer mechanism for different metatarsal geometries: a finite element study," Journal of biomechanical engineering, vol. 131, p. 021011, 2009.

[24] Christian. Cifuentes-De la Portilla, Ricardo. Larrainzar-Garijo, and Javier. Bayod, "Biomechanical stress analysis of the main soft tissues associated with the development of adult acquired flatfoot deformity," Clinical Biomechanics, vol. 61, no. c, pp. 163 - 171, dec 2018.

[25] Christian Cifuentes-De la Portilla, Ricardo Larrainzar-Garijo, and Javier Bayod, "Analysis of the main passive soft tissues associated with adult acquired flatfoot deformity development: A computational modeling approach," Journal of Biomechanics, 2019.

[26] Timothy A. Burkhart, David M. Andrews, and Cynthia E. Dunning, "Finite element modeling mesh quality, energy balance and validation methods: A review with recommendations associated with the modeling of bone tissue," Journal of biomechanics, vol. 46, pp. 1477-1488, 2013.

[27] Lijun Wu, "Nonlinear finite element analysis for musculoskeletal biomechanics of medial and lateral plantar longitudinal arch of Virtual Chinese Human after plantar ligamentous structure failures," Clinical Biomechanics, vol. 22, pp. 221-229, 2007.

[28] Joseph M. Mansour, "Biomechanics of cartilage," Kinesiology: the mechanics and pathomechanics of human movement, pp. 66-79, 2003.

[29] J. Bayod, R. Becerro-de-Bengoa-Vallejo, M. E. Losa-Iglesias, and M. Doblaré, "Mechanical stress redistribution in the calcaneus after autologous bone harvesting," Journal of biomechanics, vol. 45, pp. 1219-1226, 2012.

[30] G. A. Arangio and E. P. Salathe, "A biomechanical analysis of posterior tibial tendon dysfunction, medial displacement calcaneal osteotomy and flexor digitorum longus transfer in adult acquired flat foot.," Clinical Biomechanics, vol. 24, no. 4, pp. 385-390, 2009.

[31] J. T. Deland et al., "Posterior tibial tendon insufficiency results at different stages.," HSS journal, vol. 2, pp. 157-160, 2006.

[32] Kai Tao et al., "An in vivo experimental validation of a computational model of human foot," Journal of Bionic Engineering, vol. 6, pp. 387-397, 2009.

[33] R. Larrainzar-Garijo, C. Cifuentes-De la Portilla, B. Gutiérrez-Narvarte, E. Díez-Nicolás, and J. & Bayod, "Efecto de la osteotomía medializante de calcáneo sobre tejidos blandos de soporte del arco plantar: un estudio computacional," Revista Española de Cirugía Ortopédica y Traumatología., vol. 4, no. 3, 2018.

[34] Amit Gefen, Michal Megido-Ravid, Yacov Itzchak, and Mircea Arcan, "A 3-D numerical model of the human foot structure during gait," in [Engineering in Medicine and Biology, 1999. 21st Annual Conference and the 1999 Annual Fall Meetring of the Biomedical Engineering Society] BMES/EMBS Conference, 1999. Proceedings of the First Joint, vol. 1, 1999, p. 559.

[35] Jason Tak-Man Cheung, Ming Zhang, Aaron Kam-Lun Leung, and Yu-Bo Fan, "Three-dimensional finite element analysis of the foot during standing—a material sensitivity study," Journal of biomechanics, vol. 38, pp. 1045-1054, 2005.

[36] Zhongkui Wang, Kan Imai, Masamitsu Kido, Kazuya Ikoma, and Shinichi Hirai, "Study of Surgical Simulation of Flatfoot Using a Finite Element Model," in Innovation in Medicine and Healthcare 2015.: Springer, 2016, pp. 353-363.

[37] Z. Wang, M. Kido, K. Imai, K. Ikoma, and S & Hirai, "Towards patient-specific medializing calcaneal osteotomy for adult flatfoot: a finite element study," Computer methods in biomechanics and biomedical engineering, vol. 21, no. 4, pp. 332-343, 2018.

[38] D. H. Zanolli, R. R. Glisson, J. A. Nunley, and M. E. & Easley, "Biomechanical assessment of flexible flatfoot correction: comparison of techniques in a cadaver model," JBJS, vol. 96, p. 45, 2014.

[39] I. D. Hutchinson et al., "How do hindfoot fusions affect ankle biomechanics: a cadaver model," Clinical Orthopaedics and Related Research, vol. 474, no. 4, pp. 1008-1016, 2016.

[40] KJ Logel, BG Parks, and LC Schon, "Calcaneocuboid distraction arthrodesis and first metatarsocuneiform arthrodesis for correction of acquired flatfoot deformity in a cadaver model," Foot Ankle Int, vol. 28, no. 4, pp. 435 - 440, 2007.

[41] Enrique Morales Orcajo, Estevam Barbosa de las Casas, and Javier Bayod López, "Computational foot modeling for clinical assessment," Universidad de Zaragoza, Ph.D. dissertation 2015.

List of Figure legends:

Figure 1: Complete FE model. All the foot tissues included in the model and the differentiation between cortical and trabecular bone are shown.

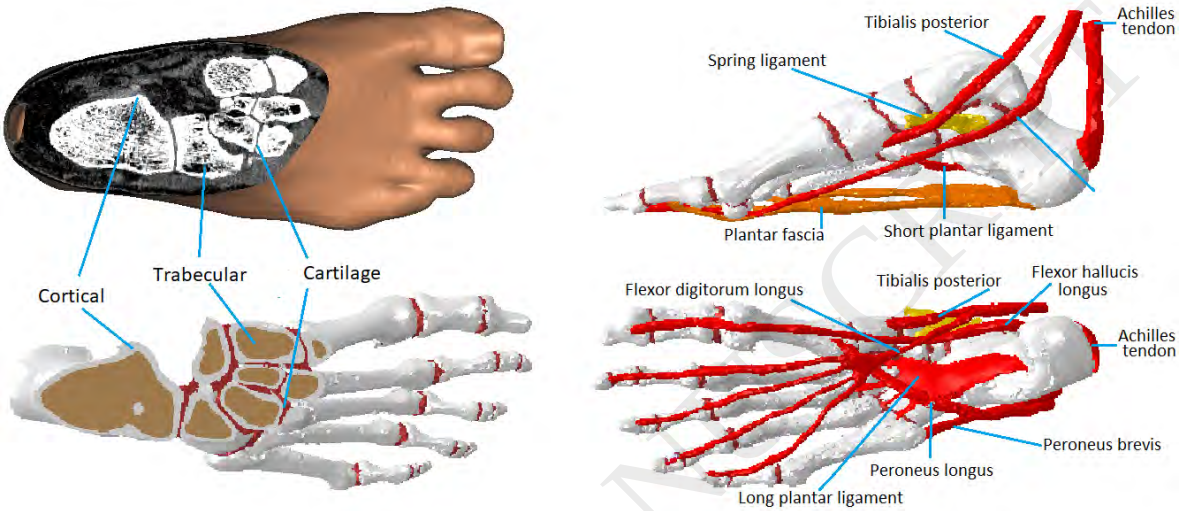

Figure 2: Explanation of how the arthrodesis was simulated. The cartilage material was changed to a cortical material in each of the fused joints.

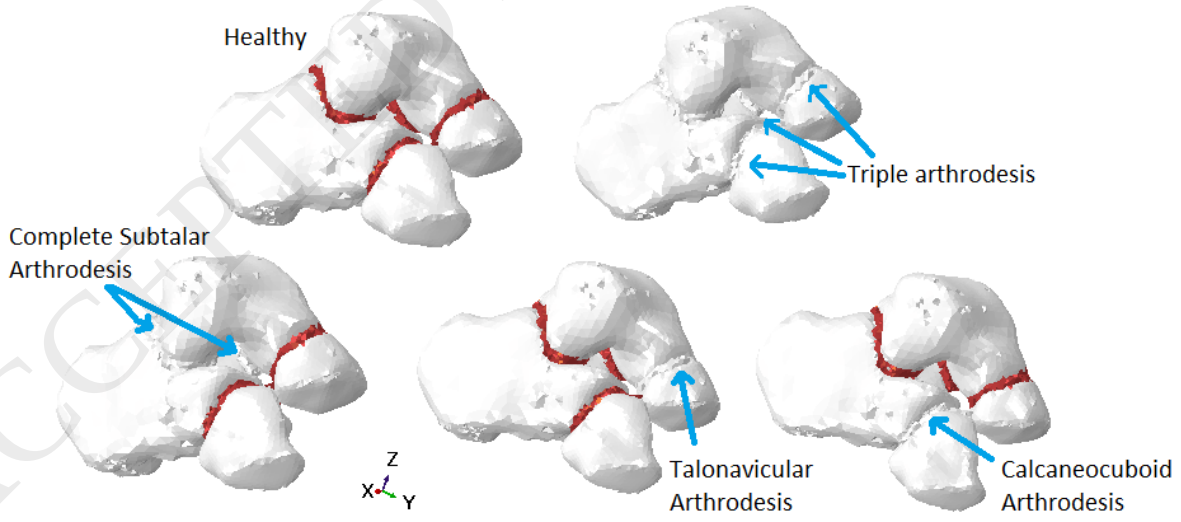

Figure 3: Boundary and loading settings applied to the foot model. The foot arch of the reconstructed model (unloaded) was measured using the internal Mourean-Costa-Bertani angle.

Figure 4: Model validation schema. Sagittal plane radiographs were used to compare the foot deformation in two loading conditions (light loading and normal standing load).

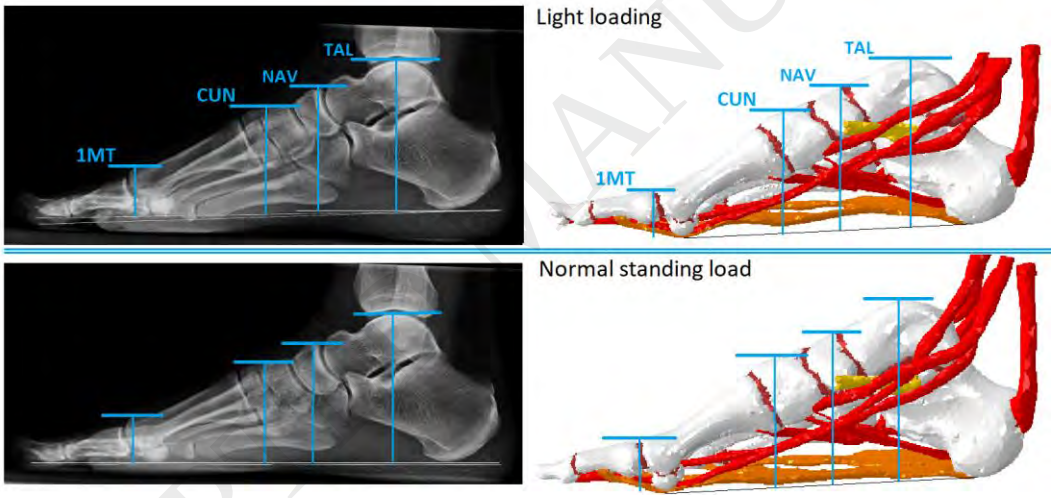

Figure 5: Structural deformation obtained after simulating both the healthy foot and the Adult acquired flatfoot deformity case.

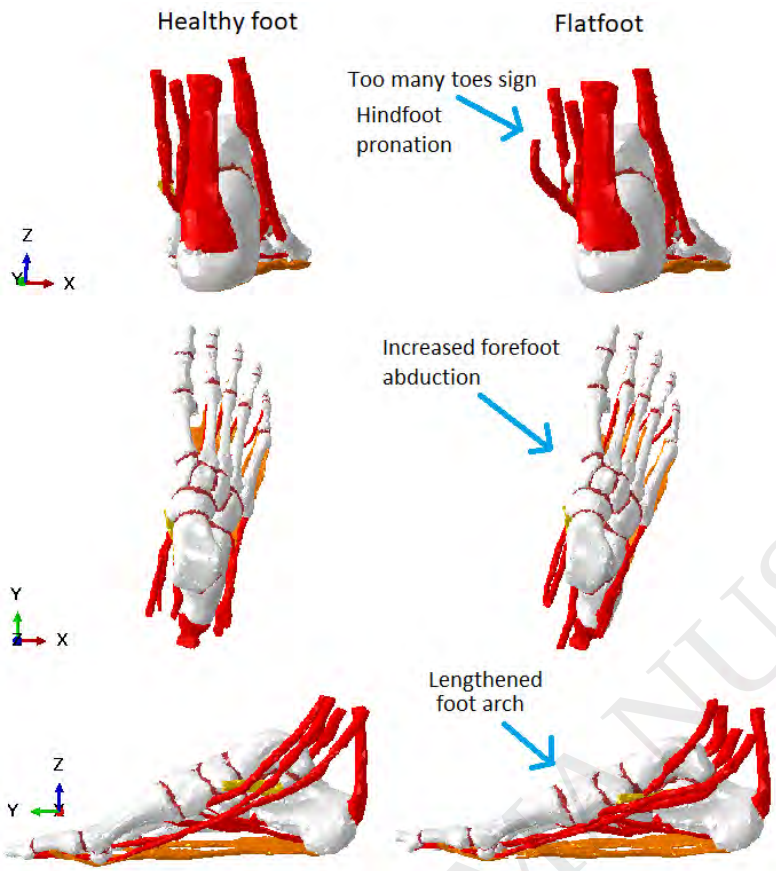

Figure 6: Plantar fascia biomechanical stress (N/mm^2) generated after simulating a tibialis posterior tendon dysfunction.

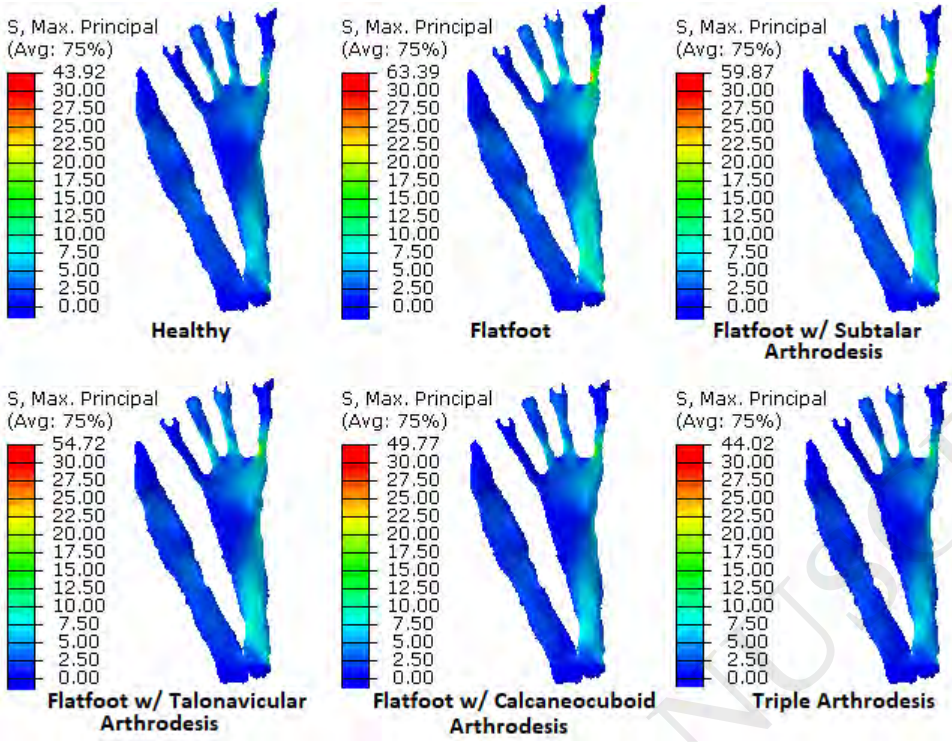

Figure 7: Spring ligament biomechanical stress (N/mm^2) generated after simulating a tibialis posterior tendon dysfunction.

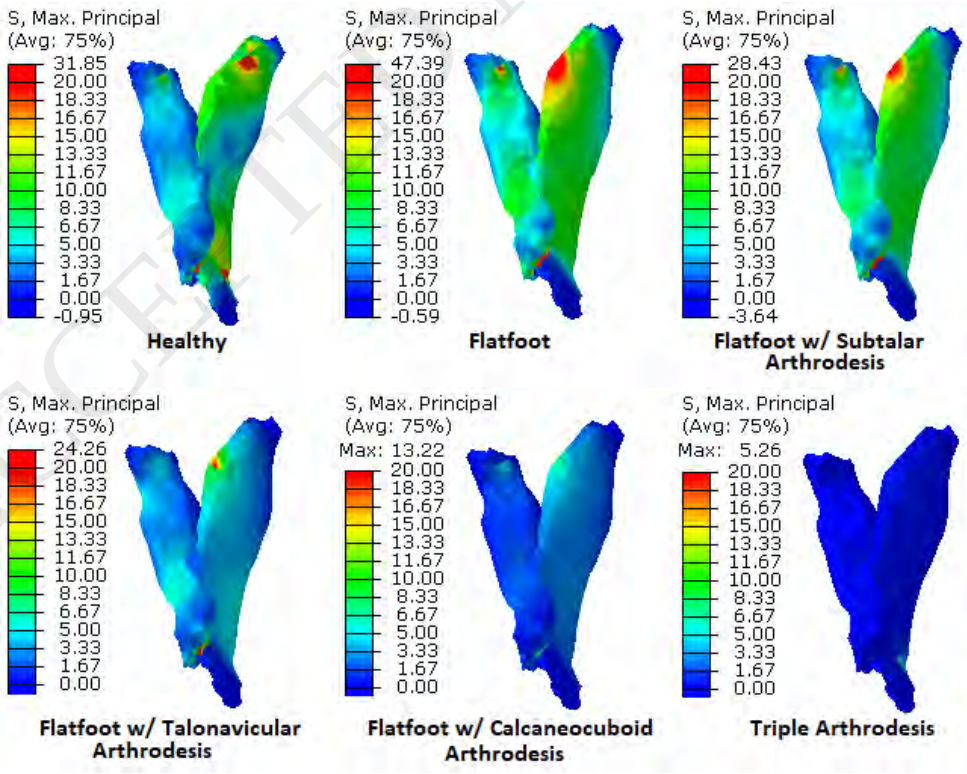

Figure 8: Maximum principal stress (N/mm^2) generated on the hindfoot bones (Calcaneus, Talus, Cuboid and Navicular), after simulating a plantar fascia, spring ligament and tibialis posterior tendon dysfunction.

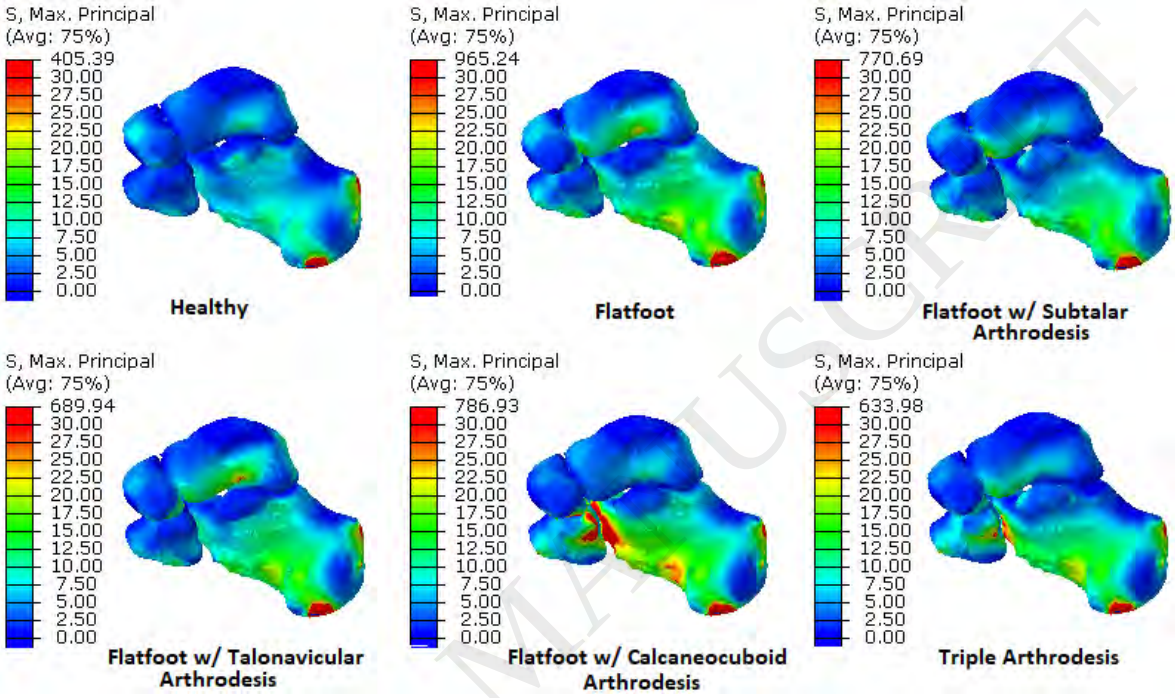

Figure 9: Maximum principal stress (N/mm^2) generated on forefoot bones (Metatarsals and phalanges) after simulating a plantar fascia, spring ligament and tibialis posterior tendon dysfunction.

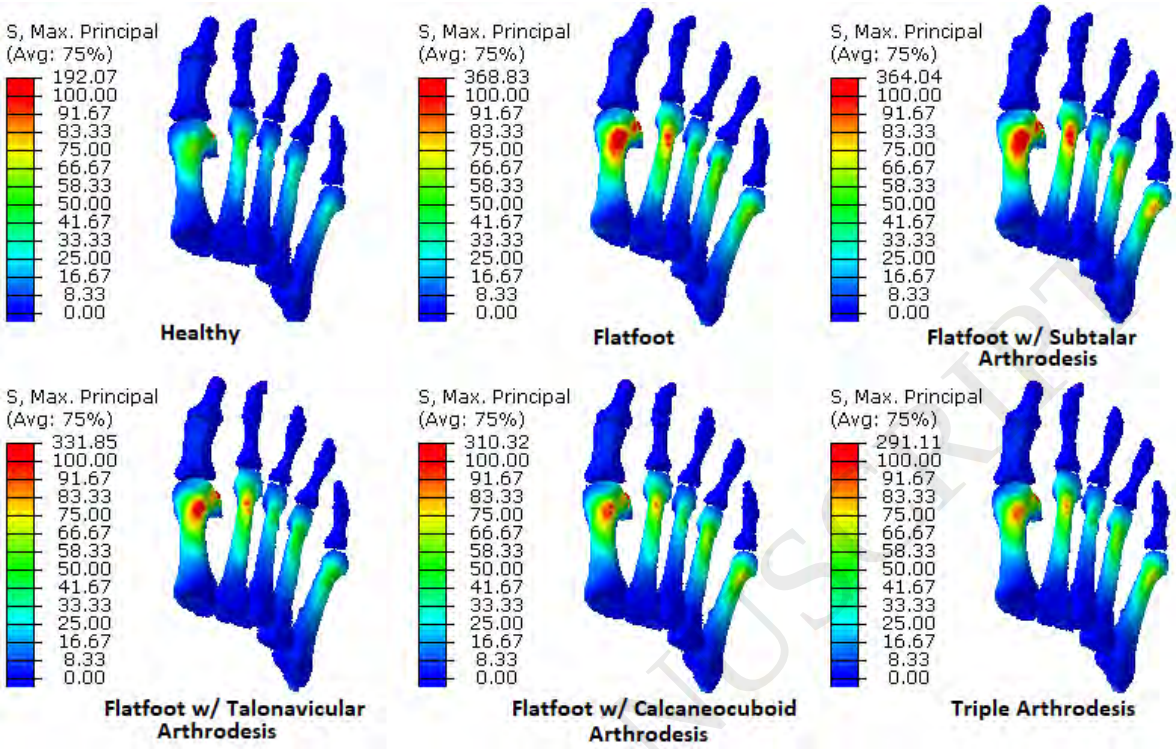

Table 1: Summary of the mesh quality measures, following the recommendations of Burkhart et al. [26], also used by Morales et al [41].

Evaluation metrics	Criteria	Accurate elements	Inaccurate elements
Element jacobians	> 0.2	99.99%	0.01%
Aspect ratio	< 3	93.5%	5,5%
Min. Angles	> 30°	100%	0%
Max. Angles	< 120°	100%	0%

Table 2: Results of the validation process. The values represent the difference between each reference point measured in two loading scenarios.

Reference point	Model prediction (mm)	Patient average (mm)
TAL	- 0.337	- 0.33 (± 0.139)
NAV	- 0.28	- 0.258 (± 0.039)
CUN	- 0.25	- 0.192 (± 0.077)
1MT	- 0.065	- 0.078 (± 0.031)

Table 3: Maximum stress (N/mm^2) generated after simulating a tibialis posterior tendon dysfunction.

	Healthy	Flatfoot	Subtalar arthrodesis	Talonavicular arthrodesis	Calcaneocuboid arthrodesis	Triple arthrodesis
SPL	24,88	28,92	27,18	26,1	3,8	2,75
LPL	24,42	35,51	36,66	28,69	64,19	57,87
PBT	210,77	207,77	209,67	208,89	215,13	216,70
PLT	183,76	246,2	252,17	237,6	312,7	328,9
FHL	242,7	247,6	228	225,42	243,9	271,9
FDL	184,3	191,16	185,18	185,49	191,03	183,89
AT	104,1	105	105	105	110	109

Table 4: Maximum stress (N/mm^2) generated after simulating a plantar fascia, spring ligament and tibialis posterior tendon dysfunction.

	Healthy	Flatfoot	Subtalar arthrodesis	Talonavicular arthrodesis	Calcaneocuboid arthrodesis	Triple arthrodesis
SPL	24,88	42,34	39,50	34,98	4,61	3,38
LPL	24,42	60,67	64,62	41,53	82,33	72,2
PBT	210,77	210,41	178,91	213,9	219,73	221,58
PLT	183,76	247,34	241,9	213,75	382,56	354,93
FHL	242,7	267,2	243,3	247,36	248,09	252,27
FDL	184,3	182,27	166,12	183,97	183,67	179,16
AT	104,1	136	121	114	114	112